Chemical Engineering Journal 237 (2014) 291–299

Contents lists available at ScienceDirect

Chemical Engineering Journal

journal homepage: www.elsevier.com/locate/cej

A facile method to produce graphene oxide-g-poly(L-lactic acid) as an promising reinforcement for PLLA nanocomposites

Wenxiao Li, Zhiwei Xu *, Lei Chen, Mingjing Shan, Xu Tian, Caiyun Yang, Hanming Lv, Xiaoming Qian

Key Laboratory of Advanced Braided Composites, Ministry of Education, School of Textiles, Tianjin Polytechnic University, Tianjin 300387, People's Republic of China

HIGHLIGHTS

- GO grafted with PLLA (GO-*g*-PLLA) was synthesized by in situ polycondensation.
- The weight percent of PLLA chains in obtained GO-*g*-PLLA was as high as 30.8%.
- The mechanical property of PLLA/GO-*g*-PLLA composites was enhanced significantly.
- It is owing to the improvement of interfacial adhesion between GO-g-PLLA and PLLA.

GRAPHICAL ABSTRACT

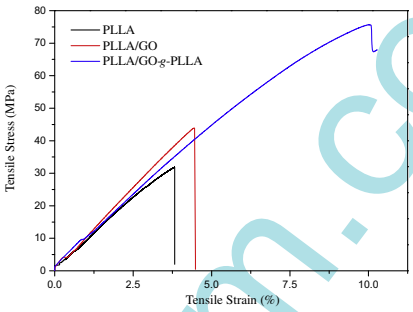

ARTICLE INFO

Article history:
Received 28 May 2013
Received in revised form 7 September 2013
Accepted 10 October 2013
Available online 22 October 2013

Keywords:
Functionalized graphene oxide
Poly(L-lactic acid)
Polycondensation
Nanocomposites
Mechanical properties

ABSTRACT

Poly(L-lactic acid) (PLLA) nanocomposites reinforced with graphene oxide (GO) or GO grafted with PLLA (GO-*g*-PLLA) were prepared by solution blending and then compression molding method, where GO-*g*-PLLA was synthesized via one step based on in situ polycondensation of the L-lactic acid monomers initiated by lyophilized GO. The average thickness of GO was increased by about 2 nm and the weight percent of grafted PLLA chains in obtained GO-*g*-PLLA was as high as 30.8%. It was clearly evidenced that the functionalization of GO with this method enhanced its dispersion and interfacial interactions with the PLLA matrix and thus improved the final thermostability and mechanical properties of nanocomposites. The flexural and tensile strength of PLLA/GO-*g*-PLLA nanocomposites were increased by 114.3% and 105.7%, respectively, compared with neat PLLA.

1. Introduction

Compared with traditional composites, polymer nanocomposites exhibit dramatic changes in some properties at very low loadings (generally ⩽2 wt%) of nanofillers like cellulose nanofibers [1], carbon nanotubes [2], graphite nanoplatelets [3–5], and nanoclays [6]. However, the optimal performance conferred by these nanofillers can be achieved only when the homogeneous dispersion of nanofillers and strong interfacial adhesion between nanofillers and polymer matrix are realized. Graphene, a single-atom-thick sheet of hexagonally arrayed sp^2-bonded carbon, chemically similar to carbon nanotubes and structurally analogous to silicate layers [7], has drawn the attention of researchers in various fields due to its remarkable mechanical, thermal [8], and electrical properties [9]. With such outstanding properties, graphene nanosheets can be usefully applied as a reinforcing material in polymers using a variety of methods including solution (or melt) blending [3,10,11] and in situ polymerization [12]. However, to improve the solubility of graphene nanosheets in various organic and aqueous solvents, as well as their miscibility with polymer materials, the preparation of graphene derivatives by chemical modification has been the subject of intense interest recently [13,14].

Poly(L-lactic acid) (PLLA), an aliphatic polyester produced from renewable biomasses such as corn and sugar beet, has been recently spotlighted as a biodegradable, sustainable, and eco-friendly

* Corresponding author. Tel./fax: +86 022 83955231.
E-mail address: xuzhiwei@tjpu.edu.cn (Z. Xu).

1385-8947/$ - see front matter © 2013 Elsevier B.V. All rights reserved.
http://dx.doi.org/10.1016/j.cej.2013.10.034

substituent for petroleum-based polymers [15,16]. PLLA has balanced properties of mechanical strength, thermal plasticity and transparency [17]. Nevertheless, its crystallization rate, thermal and mechanical properties need to be improved for long-term high performance applications [18]. Many reports have verified that the addition of functionalized carbon nanomaterials can increase the crystallization rate, and promote the thermal stability and mechanical strength of PLLA. For instance, Cao and co-workers [19] made successful use of lyophilized graphene nanosheets to improve the mechanical and thermal properties of PLLA in some degree. The graphene nanosheets were in the form of chemically reduced graphene oxide which were prepared by a modified Hummers method and then chemically reduced with hydrazine. Yang et al. [20] prepared a series of PLLA/thermally reduced graphene oxide composites via the in situ ring-opening polymerization of lactide, using thermally reduced graphene oxide as the initiator. The thermal stability, crystallization rate and electrical conductivity of PLLA were increased. Although in situ polymerization is an effective way to disperse the fillers in the matrix uniformly and generate better interfacial interactions with the host polymer, the synthesis of high molecular weight PLLA requires severe conditions [21] and expensive precursor (lactide) [22]. In the works of Song et al. [23] and Yoon et al. [24], PLLA was successfully covalently grafted onto the convex surfaces and tips of the multi-walled carbon nanotubes (MWNTs) via one step based on in situ polycondensation of the commercially available L-lactic acid monomers. They prepared MWCNTs with carboxylic functional groups (MWCNTs–COOH) via a mixture of concentrated sulfuric and nitric acids oxidation. Subsequently, the MWCNTs–COOH acted as an initiator, and PLLA was grafted onto the MWCNTs–COOH surface. The resulting MWNTs-*g*-PLLA were mixed with commercially available neat PLLA to prepare PLLA/MWCNTs-*g*-PLLA nanocomposites and improved the initial modulus, tensile strength and crystallization rate of PLLA. Graphene oxide (GO) has a higher content of oxygen-containing functional groups [25,26] and higher specific surface area [27] than MWCNTs–COOH, thus it is expected to be more promising than MWCNTs–COOH in polycondensation of L-lactic acid. Besides, the preparation of GO is based on a frequently-used method to prepare graphite oxide by using strong oxidizing agents, which is then exfoliated to single or few platelets via sonication in water [19,28], without any other further treatment. But the facile one-step polycondensation method has not been applied to the functionalization of GO. It is desirable to use GO as the reactants or initiators in the in situ polymerization of L-lactic acid monomers to prepare GO grafted with PLLA (GO-*g*-PLLA). Moreover, the grafted polymer chains can also act as compatibilizer when graphene sheets are mixed with polymer, particularly when they are of the same nature as matrix, which can improve the interfacial adhesion and maximize the compatibility between the partners [29,30]. So it is estimated that GO-*g*-PLLA would exhibit excellent performance in the reinforcement of PLLA.

We herein described an in situ polycondensation approach, to functionalize the pristine GO with PLLA via one step from commercially available polycondensation-type monomers, L-lactic acid, as shown in Scheme 1. In our work, in order to prevent GO aggregation, we used lyophilization method to prepare GO powder, which was shown to be extremely light and macroporous, so that the functionalization of GO was facilitated and its dispersibility with polymer was improved [31]. GO-*g*-PLLA was successfully prepared judging from the results of Fourier transform infrared spectroscopy (FTIR) , X-ray photoelectron spectroscopy (XPS), thermogravimetric analysis (TGA) and atomic force microscopic (AFM), and it was proved that the oxygen-containing functional groups on GO could initiate the polycondensation reaction of L-lactic acid. In addition, we prepared neat PLLA, PLLA/GO and PLLA/GO-*g*-PLLA nanocomposites by solution blending and compression molding and then made a comparative study on these three samples to clarify the important role of PLLA chains on GO surface in the enhancement of host polymer.

2. Experimental

2.1. Materials

Natural graphite powder was provided by Nanjing Xianfeng Nanomaterial Science and Technology Co., Ltd., China. PLLA (biopla 6202F) was purchased from Ningbo Global Biological Material Co., Ltd. Its number-average molecular weights is $Mn = 1.1 \times 10^5$ g/mol.

L-lactic acid [$CH_2O(CH_3)COOH$] (85 wt% aqueous solution) was purchased from Tianjin Reagents Co., Ltd., which was dehydrated with magnetic stirring for 8 h at 110 °C under a vacuum distillation unit to remove the water before used as the monomer for polycondensation. Potassium permanganate ($KMnO_4$), sulfuric acid (H_2SO_4, 98%), phosphoric acid (H_3PO_4), hydrogen peroxide (H_2O_2), and Tin octoate ($Sn(oct)_2$) of reagent grade were purchased from Tianjin Reagents Co., Ltd. These chemicals were used as received.

2.2. Preparation of GO

Graphite oxide was synthesized from commercial graphite powder according to a improved Hummer's method [25]. In detail, a 9:1 mixture of concentrated H_2SO_4/H_3PO_4 (360:40 mL) is added to a mixture of graphite flakes (3.0 g, 1 wt equiv.) and $KMnO_4$ (18.0 g, 6 wt equiv.), and then the mixture was stirred for 12 h at 50 °C. After that it was poured into ice water (400 mL) with 30% H_2O_2 (3 mL) and stood for one night. The resultant product was washed on the centrifuge until the pH value of the supernatant fluid became 7 and then was dried in a vacuum oven at 45 °C forming graphite oxide powder.

The solid was suspended in deionized water (1 mg/mL) and sonicated for 2.5 h [28,32] to generate a GO suspension. Subsequently, the aqueous GO suspension was frozen into an ice cube in a refrigerator (−15 °C) for 8 h and then was freeze-dried using a FD-1A-50 lyophilizer (Boyikang Co., Ltd., China) with a condenser temperature of −50 °C at a inside pressure of less than 20 Pa. After 48 h lyophilization and 48 h vacuum drying (45 °C) process, low-density, loosely packed GO powder was finally obtained.

2.3. Preparation of GO-g-PLLA

To prepare GO-*g*-PLLA by melt polycondensation, GO (1.0 g) was mixed with dehydrated L-lactic acid (200 mL). The mixture was sonicated for 30 min to obtain a homogeneous dispersion of GO in the L-lactic acid. Then, $Sn(oct)_2$ (0.2 g) as the polycondensation catalyst was added into the viscous mixture. Melt-polycondensation of L-lactic acid with GO was carried out in 500-mL Florence flask for 5 h at 180°Cwith magnetic stirring under vacuum. The internal pressure in the polymerization reactor was about 100 Pa. The scheme of melt-polycondensation to prepare GO-*g*-PLLA is shown in Scheme 1. After melt-polycondensation, the final product was dissolved in excess chloroform and then filtered through the PTFE membrane to remove the unreacted monomer, PLLA homopolymer and PLLA ungrafted to graphene nanosheets [23,29]. The dissolution and filtration process were repeated several times until no PLLA in the filter liquor could be detected. The resulting solid was dried for 24 h at 50 °C under vacuum to obtain GO-*g*-PLLA.

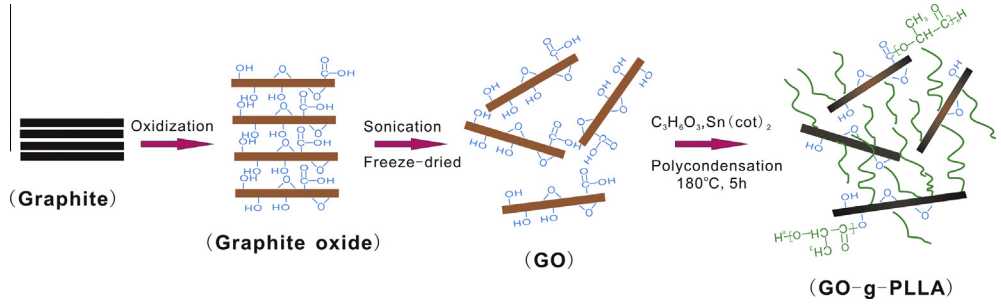

Scheme 1. Schematic illustration for the preparation and functionalization of GO.

2.4. Preparation of PLLA/GO-g-PLLA nanocomposites

A predetermined amount of GO-*g*-PLLA (0.5 wt%) was added to 200 mL chloroform and sonicated for 2 h, and then 20 g PLLA was added into the chloroform solutions, subsequently mixing for 3 h with mechanical stirring. The mixed solution of PLLA and GO-*g*-PLLA was sonicated for another 2 h and then poured into excess methanol and filtered through a vacuum filter. Finally, the dried PLLA/GO-*g*-PLLA composites were obtained as a gray-to-black solid by drying it in a vacuum oven at 55 °C for 48 h. In order to test the mechanical properties of the composites, rectangular samples were prepared by compression molding. The mold (100 mm × 100 mm × 1 mm) filled with the composite pellets was placed in hot press which was preheated at 170 °C. A pressure of 20 MPa was applied for 2 min to soften the pellets and then a pressure of 40 MPa was applied for 10 min. Finally, the mold was quenched to 30 °C with the cooled water recycle system and removed from the hot press to obtain a composite panel with 1 mm thickness. For comparison, PLLA and PLLA/GO (0.5 wt%) sheets were also prepared by the same method.

2.5. Instruments and characterization

FTIR, XPS and TGA were conducted to show the change of chemical character of GO and GO-g-PLLA. FTIR (Bruker Tensor 27) spectra were recorded from 600 to 4000 cm^{-1} with a resolution of 2 cm^{-1} and 32 scans. XPS measurements were performed using a PHI 5700 ESCA System Auger electron spectrometer (Physical electronics company, America) equipped with a hemispherical electron analyzer and a scanning monochromatic Al Kα ($h\nu$ = 1486.6 eV) X-ray source. TGA curves were obtained from a Mettler SDTA851e. The samples were heated from 25 °C to 800 °C at a rate of 10 °C/min in an aluminum crucible under 50 mL/min of nitrogen purging. Molecular weight of free PLLA was determined by a gel permeation chromatograph (GPC) on a Waters 1525 apparatus, USA. AFM (Digital Instrument CSPM5500) measurements with the typical contact-mode were performed to observe the morphology of GO and GO-*g*-PLLA.

The particle size distributions of GO and GO-g-PLLA in the chloroform were tested using a dynamic light scattering (DLS) system (Delsa Nano C, Beckman Coulter Co., Ltd., USA) with equivalent sphere model. The morphology and dispersion of graphene nanosheets in the matrix were evaluated by a field-emission scanning electron microscope (FE-SEM) (JSM-6700F, accelerating voltage 10.0 kV). The tensile fractured surfaces of test specimens were sputter-coated with gold before the FE-SEM observations to avoid charging.

The crystallization behaviors of PLLA and nanocomposites were measured by a differential scanning calorimeter (DSC), DSC Q200 V23.10 Build 79, in a nitrogen flow (50 mL/min) with a heating rate of 10 °C/min, spanning the temperature range from 40 °C to 200 °C. Dynamic mechanical analysis (DMA) was carried out in DMA/SDTA861e in the single cantilever beam mode at 1 Hz, in the range of temperature from 40 °C to 100 °C. Sample dimensions used were 20.0 mm × 10.0 mm × 1.0 mm (length, width and thickness, respectively). The mechanical properties of the nanocomposites were evaluated by flexural tests and tensile tests, which were both performed on a universal mechanical testing machine (MTI INSTRON). Flexural tests of the PLLA composites were determined by three point bending tests (50.8 mm × 12.7 mm × 1 mm) according to ASTM D790 standard with a cross-head speed at 1.27 mm/min and a span at 25.4 mm, to obtain flexural strength and ultimate strain. Tensile property of the nanocomposites (80 mm × 10 mm × 1 mm) were performed according to GB 13022 standard at a crosshead speed of 5 mm/min. Five different measurements were carried out for each sample.

3. Results and discussion

3.1. Characterization of GO and GO-g-PLLA

The FTIR spectra of PLLA, GO and GO-*g*-PLLA were displayed in Fig. 1. In GO (Fig. 1b), the characteristic features were the band at 3430 cm^{-1} (O—H stretching vibrations), 1728 cm^{-1} (C=O stretching vibrations from carboxylic groups) and 1632 cm^{-1} (skeletal vibrations from unoxidized graphitic domains) [25,33–36]. For GO-*g*-PLLA, more intense C=O stretching bands appeared at 1750 cm^{-1}. The wave number of C=O stretching band shifted upward from 1728 cm^{-1} (GO) to 1750 cm^{-1} (GO-*g*-PLLA), which could be explained by the fact that the band at 1728 cm^{-1} of GO corresponds to the carboxylic acid groups, while the band at 1750 cm^{-1} of GO-*g*-PLLA corresponds to the ester groups of PLLA chains (Fig. 1a and c) [15,23]. In addition, the intensity of band at 3430 cm^{-1} which corresponded to hydroxyl groups decreased clearly because the PLLA chains were grafted to GO surface (the esterification reaction between carboxylic groups or hydroxyl groups on L-lactic acid and hydroxyl groups or carboxylic groups on GO) [29]. The resonances due to C—CH_3 stretching mode,

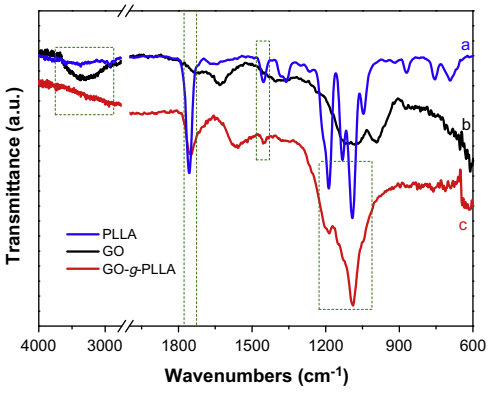

Fig. 1. FTIR spectra of (a) PLLA, (b) GO and (c) GO-*g*-PLLA.

—CH_3 rocking mode and —CH_3 asymmetric bending mode of PLLA were at 1080, 1185, and 1453 cm^{-1}, respectively [23,24,37–39]. Therefore, GO could be served as an initiator for the polycondensation of the commercially available L-lactic acid monomers and PLLA chains were successfully grafted on GO.

The functionalization of GO with L-lactic acid was also confirmed by XPS. The C1s core-level spectra of both samples were presented in Fig. 2. The spectrum of GO (Fig. 2a) consisted of five components, namely C=C/C—C (284.8 eV), C—OH (285.3 eV), C—O (286.3ev), C=O (288.0 eV) and O—C=O (289.1 eV) [32,40]. After functionalization with PLLA, the —OH of GO was reduced and the C—H and O—C=O of GO-*g*-PLLA corresponding to PLLA [20] were increased significantly. According to many studies of the polycondensation reaction mechanism of lactic acid [23,41,42], this reaction is considered to involve both "grafted from" and "grafted to" approaches. The "grafted from" approach means that the monomers are in situ polymerized from the initiators or catalysts on GO surface [43]. The "grafted to" approach means that GO is bonded with existing macromolecules whose terminal functional groups react with the functional groups on GO [44]. In this reaction system, the L-lactic acid monomer reacted with carboxyl acid and hydroxyl groups on the surface of GO, which is attributed to "grafted from" approach, and at the same time the formed free L-lactide or tripolymer coupled with the function groups supported by the surface of GO, which is attributed to "grafted to" approach. As the polymerization went on, the surface of GO was almost coated with a layer of PLLA chains, which made it much more difficult for free oligomer to hit the surface of GO than the terminal groups of grafted PLLA chains due to high steric hindrance. Therefore, during this stage the chain length of PLLA chains was continuously increased. Besides, the —OH reacted with the $Sn(oct)_2$ to form $R_{initiator}$—C—O—Sn which would initiate the chain growth, and the chemical structure might be $R_{initiator}$—C—O—R'_{PLLA}. Furthermore, the C/O ratio of GO decreased from 2.22 to 1.67 after grafting PLLA due to the higher content of oxygen of PLLA than GO.

The grafted polymer content in GO-*g*-PLLA was tested by TGA. As shown in Fig. 3, the weight loss stage of GO was range of 70–230 °C. The weight loss found for GO at the temperature range from 70 to 130 °C was due to the evaporation of physically absorbed water and the weight loss at range from 130 to 230 °C was attributed to pyrolysis of the oxygen-containing functional groups, yielding CO, CO_2 and water vapor [36,45]. However, there were two clearly separated weight loss stages in the range of 100–160 °C and 270–400 °C for GO-*g*-PLLA, which corresponded to the loss of oxygen-containing functional groups on GO and grafted PLLA chains [20,23], respectively. It seemed that the weight loss of GO-*g*-PLLA was increasing continuously after 400 °C (Fig. 3b). However, PLLA had been decomposed completely before 400 °C as seen in Fig. 3c and other researches [30,46]. So the content of PLLA grafted to GO was about 30.8 wt%, corresponding to the weight loss of the degradation of PLLA. The small weight loss

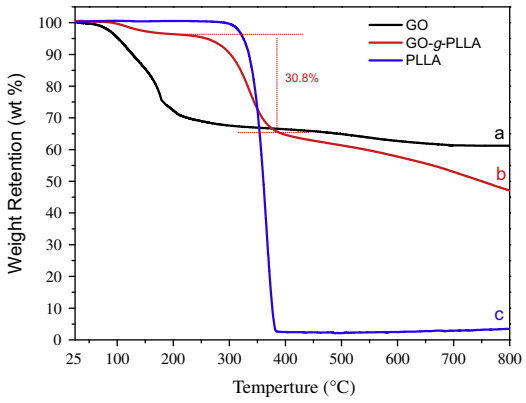

Fig. 3. Thermal degradation curves of (a) GO, (b) GO-*g*-PLLA and (c) PLLA. Scanning rate 10 °C/min.

of GO-*g*-PLLA after 400 °C might be caused by the decomposition of the treated GO [47] or other impurity. The molecular size of PLLA grafted on GO was determined by measuring the free PLLA which was simultaneously produced during functionalization [48,49]. GPC results demonstrated that the number-average molecular weight was 3528 g/mol and the polydispersity index is 1.04.

On the other hand, in the preparation of GO-*g*-PLLA, 1 g of GO was mixed with 200 mL of L-lactic acid (the weight percentage of GO was around 0.42%), but after reaction the quality of GO was around 69.2 wt%. The resulting PLLA grafted on the GO only accounted for less than one percent of L-lactic acid. Because the content of grafting PLLA increased with the feed ratio of monomer to GO in a certain scope [36,50], we chose a high ratio in this feed. Considering the efficiency of reaction, the optimal proportion of monomer to GO requires further discussion in our future work.

AFM images are used to observe the morphology and the thickness of GO and GO-*g*-PLLA. Fig. 4a showed that the thickness of GO was about 1.37 nm, which was consistent with the reported values [8]. After in situ polycondensation, the thickness of GO-*g*-PLLA was about 3.23 nm (as shown in Fig. 4b). The great increase of thickness can be attributed to the PLLA chains on GO surface.

The dispersity of GO and GO-*g*-PLLA in chloroform was tested by a sedimentation experiment and a particle size analysis. As seen in Fig. 5a, both of them could form homogeneous solutions (0.5 mg/mL) after sonication for 2 h. However, GO was precipitated at the bottom after 12 h's standing, while GO-g-PLLA was still well-dispersed in the solution (Fig. 5b). This difference resulted from the grafted PLLA chains which have a strong interaction with the solvent, thus facilitating a good dispersion of GO-*g*-PLLA in chloroform.

DLS technique was also used to analyze the size and size distributions of GO and GO-*g*-PLLA. As we know, graphene nanosheets tend to aggregate back to graphite gradually due to the strong

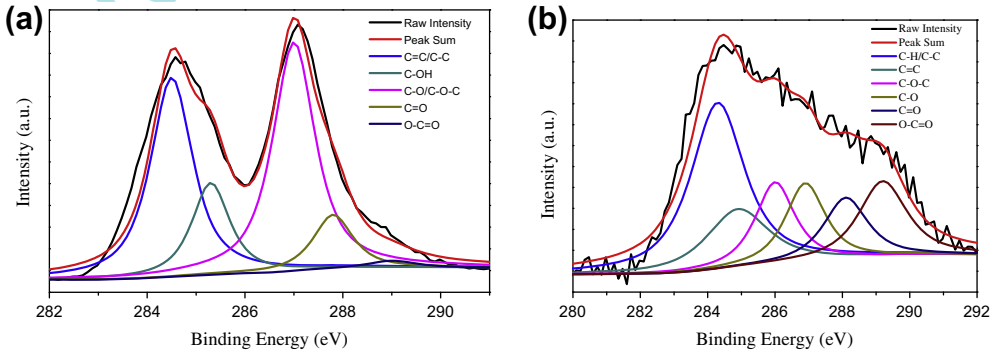

Fig. 2. The C1s peak in the XPS spectra of (a) GO and (b) GO-*g*-PLLA.

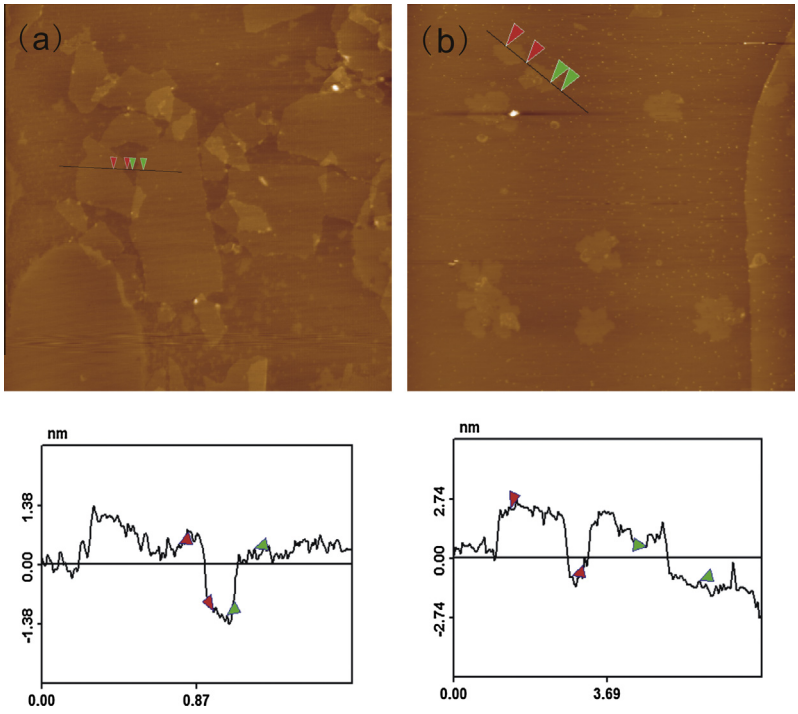

Fig. 4. Tapping mode AFM images of (a) GO and (b) GO-*g*-PLLA.

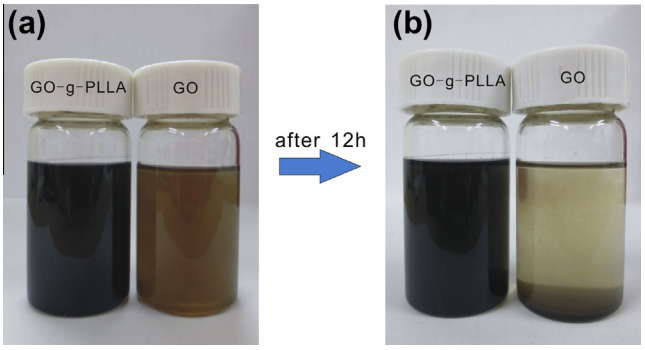

Fig. 5. (a) Photos of GO and GO-g-PLLA dispersion in chloroform (0.5 mg/mL) after sonication for 2 h; and (b) states after standing for 12 h.

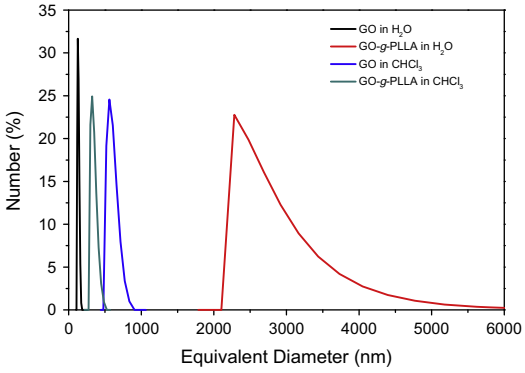

Fig. 6. Size and size distribution (in diameter, nm) detected by DLS technique of GO and GO-*g*-PLLA in water; GO and GO-*g*-PLLA in chloroform (0.5 mg/mL).

van der Waals interaction [51], therefore the size of graphene nanosheets in the solvent can reflect the dispersion state in solution. Note that here the DLS data used a sphere model to simulate graphene nanosheet assemblies and all of samples (0.5 mg/mL) were tested rapidly after sonication for 2 h. As shown in Fig. 6, the average particle size of GO in water was 126 ± 36 nm, which indicated that GO existed in the form of single- or few-layer graphene sheets and had stable distribution in water [28]. While the average particle size of GO-*g*-PLLA changed into 2798 ± 787 nm and showed wide distribution, which indicated that after treating with polycondensation, hydrophobic PLLA chains were successfully grafted on surface of GO. And thus GO-*g*-PLLA was turned into hydrophobic material and could not disperse well in water. Besides, GO and GO-*g*-PLLA showed equivalent diameters of 562 ± 210 nm and 323 ± 140 nm in chloroform, respectively. Theoretically, after grafting PLLA chains, the diameter of GO-*g*-PLLA would increase compared with GO, but due to the formation of GO aggregation in chloroform, it exhibited higher diameter and wider size distribution than GO-*g*-PLLA. Therefore, it is possible to use the way of in situ polycondensation to improve the dispersibility of GO in chloroform.

3.2. Morphology and crystallization behaviors of nanocomposites

To characterize the morphology and dispersity of fillers in the nanocomposites, FE-SEM images of fracture surfaces of PLLA, PLLA/GO and PLLA/GO-*g*-PLLA composites were examined, as displayed in Fig. 7. The PLLA showed a smooth fracture surface morphology (Fig. 7a). For PLLA/GO nanocomposites, GO formed agglomeration in the PLLA matrix and floated on the PLLA matrix, as marked in Fig. 7b. It is believed that GO aggregations in the PLLA matrix were caused by the Van der Waals interaction among GO as well as the poor compatibility of GO with the PLLA matrix. In the case of PLLA/GO-*g*-PLLA nanocomposites, the fracture surfaces of them were relatively crude, which indicated that more energy was required to break the composites and GO-*g*-PLLA formed strong interface with PLLA. In addition, the fracture surface of PLLA/GO-*g*-PLLA did not show noticeable GO aggregations due to the PLLA chains wrapped around GO which supported GO-*g*-PLLA to mix well with the same nature matrix. This indirectly reflected the enhanced dispersion of GO-*g*-PLLA (the solids marked by arrows in Fig. 7c might be GO-*g*-PLLA).

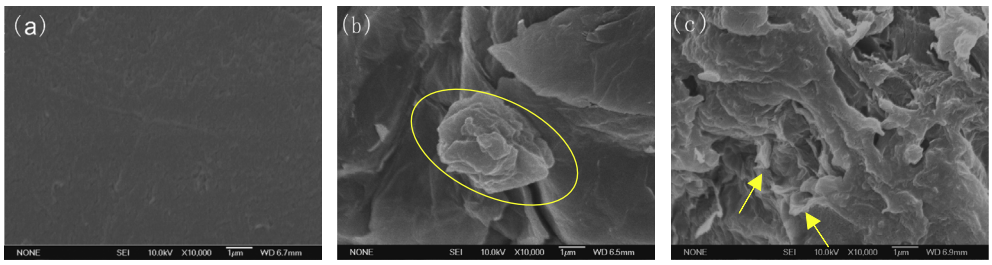

Fig. 7. Tensile fracture surface of (a) PLLA; (b) PLLA/GO; and (c) PLLA/GO-*g*-PLLA.

DSC was used to investigate the crystallization behaviors, glass transition temperature (T_g) and melting temperature (T_m) of the samples (Fig. 8). T_g and T_m of polymer are affected by the mobility of polymer chains as seen in many reports [52]. In the curve of PLLA, it showed that the T_g and T_m of PLLA were about 53.8 °C and 164.3 °C, respectively. Besides, it exhibited a double-melting behavior. In general, the first endotherm is attributed to the melting of the original crystals, and the second endotherm is owing to the crystals formed or perfected during the DSC scan [53]. With the addition of GO and GO-*g*-PLLA, T_g increased to 59.4 °C and 60.2 °C, while T_m increased to 167.1 °C and 169.1 °C, respectively. The increases of the T_g and T_m values in the nanocomposites may be ascribed to an effective attachment of PLLA to graphene derivatives, which constrained the segmental motion of the PLLA chains by mechanical interlock, hydrogen bonding and electrostatic attraction, as demonstrated in other reports [54,55]. The higher thermal stability of PLLA/GO-*g*-PLLA than PLLA/GO may reflect the higher interfacial bonding strength between PLLA and GO-*g*-PLLA.

The degree of crystallinities (χ_c) of neat PLLA and its nanocomposites is determined by the ratio of enthalpy of melting (ΔH_m) of the samples to that of 100% crystalline PLLA (ΔH_0), 93 J/g. For clarity, the temperatures of major peaks, ΔH_m and the calculated χ_c from DSC thermograms of PLLA and hybrids were summarized in Table 1. It can be seen that the incorporation of GO and GO-*g*-PLLA slightly improved crystallinities of PLLA nanocomposites. Besides, PLLA/GO and PLLA/GO-*g*-PLLA composites both showed a cold crystallization peak at about 105 °C which indicated that the addition of graphene derivatives enhanced the cold crystallization behavior.

3.3. Mechanical properties of nanocomposites

The high surface area and relatively high modulus of graphene-based materials [56] allow them to be the important load-bearing component when dispersed into polymer [13], and thus significant reinforcing effects of polymers by graphene-based fillers have been previously reported [57]. In this study, flexural and tensile tests were conducted to investigate the effect of GO and GO-*g*-PLLA on the mechanical properties of PLLA.

Table 1
T_g, T_m, crystallinity and melting enthalpy of neat PLLA and PLLA nanocomposites.

Sample	T_g (°C)	T_m (°C)	ΔH_m (J/g)	χ_c (%)
PLLA	53.8	164.3	38.9	41.8
PLLA/GO	59.4	167.1	41.0	44.1
PLLA/GO-*g*-PLLA	60.2	169.1	44.4	47.8

The dynamic mechanical properties of PLLA and nanocomposites were investigated and loss factors ($\tan\delta$), the ratio of loss modulus to storage modulus, of them were given in Fig. 9. Tan δ curves revealed one important thermal transitions corresponding to the samples, which supplied the information on the weak transition and interface of multiphase system. T_g shown in the DMA curves (taken as the peak of $\tan\delta$) was increased from 68.7 °C for PLLA to 71.3 °C (PLLA/GO) and 72.5 °C (PLLA/GO-*g*-PLLA). The values were higher than that of T_g in DSC, which was caused by the different test methods, but the trend of temperature was uniform. The shifts of T_g to high temperatures in the PLLA/GO and PLLA/GO-*g*-PLLA hybrids suggested increased adhesion between polymer and fillers in the system.

In PLLA/GO-*g*-PLLA system, the adhesion between polymer and fillers was due to the same nature of them which was bound to facilitate the chains to intertwine with each other. And thus the final mechanical interlock between polymer and nanofillers was increased.

However, why did the blend of PLLA and GO also show higher T_g and T_m, and did the interface interaction arise from the molecular interaction between PLLA and GO, i.e., hydrogen bonding? We employed the FTIR technique to verify this specific interaction because of its sensitivity to H-bonding formation. H-bonding involves C=O groups of PLLA, often regarded as H-bonding acceptor, together with —OH and —COOH groups of GO, usually regarded

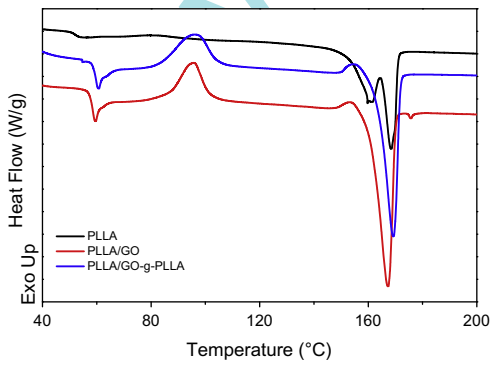

Fig. 8. DSC thermograms for the PLLA, PLLA/GO and PLLA/GO-*g*-PLLA nanocomposites.

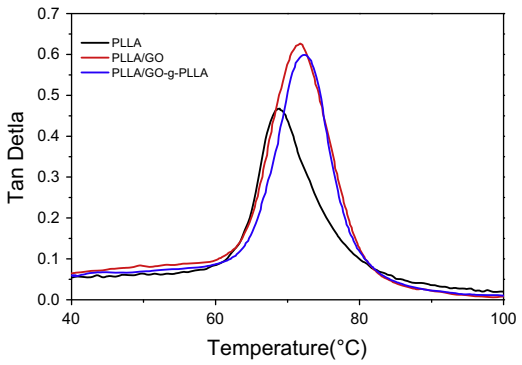

Fig. 9. Loss factor, $\tan\delta$, as a function of temperature for PLLA, PLLA/GO and PLLA/GO-*g*-PLLA.

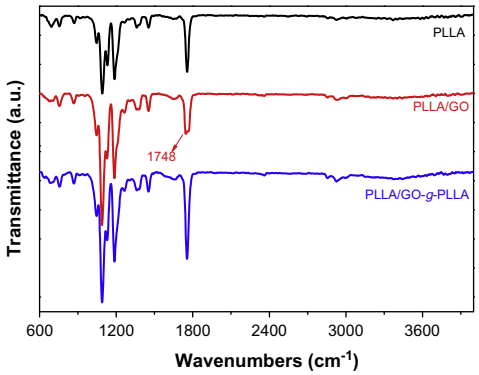

Fig. 10. FTIR spectra of PLLA, PLLA/GO and PLLA/GO-*g*-PLLA nanocomposites.

as H-bonding donor. The abundant —OH and —COOH groups on GO provided favorable condition for the formation of H-bonding. Fig. 10 showed FTIR spectra recorded at room temperature for PLLA and its blends with nanofillers. Similar FTIR bands were observed for them, except for the C=O region around 1755 cm^{-1}. In PLLA/GO, the stretching vibrations of C=O were split into two distinct peaks, unlike the single carbonyl peak of PLLA and PLLA/GO-*g*-PLLA. One of the split peaks at about 1755 cm^{-1} was still assigned to the original C=O vibration which was free and did not form H-bonding with GO; the other peak shifted to a lower wavenumber around 1748 cm^{-1}, which was caused by the formation of H-bonding, as reported in other studies [42,58]. Thus it verified the formation of H-bonding between PLLA and GO.

Flexural properties of neat PLLA, and PLLA/GO and PLLA/GO-*g*-PLLA nanocomposites were summarized in Fig. 11a. Neat PLLA used in this study has a breaking strength of about 56 MPa and a distortion at break of 1.24%. Compared with neat PLLA, PLLA/GO nanocomposites had an increased breaking strength of 109 MPa and a distortion at break of 3.02%, increasing by 94.6% and 143.5%, respectively. While PLLA/GO-*g*-PLLA nanocomposites exhibited a higher breaking strength of about 120 MPa and a distortion at break of 3.68%, increasing by 114.3% and 196.8%, respectively.

The mechanical properties of nanocomposites are significantly affected by the following factors: (i) the dispersibility of graphene-based fillers in PLLA matrix; (ii) the interfacial interaction between nanofillers and PLLA matrix; (iii) the crystallization behavior of samples. However, there was little difference in crystallinity of the three samples, as seen from the Table 1. So the difference of the mechanical properties caused by crystallinity might be ignored. Good dispersion and interfacial stress transferring lead to a more uniform stress distribution and minimize the presence of the stress concentration center [54]. In the case of PLLA/GO composites, although the sonication, mechanical stirring and rapid precipitation were used to assist the dispersibility of GO in matrix, a part of GO tended to aggregate (as seen in the Fig. 7b) due to their strong interlayer cohesive energy (van der Waals interaction) [48]. On the other hand, the oxygen-containing groups and negative

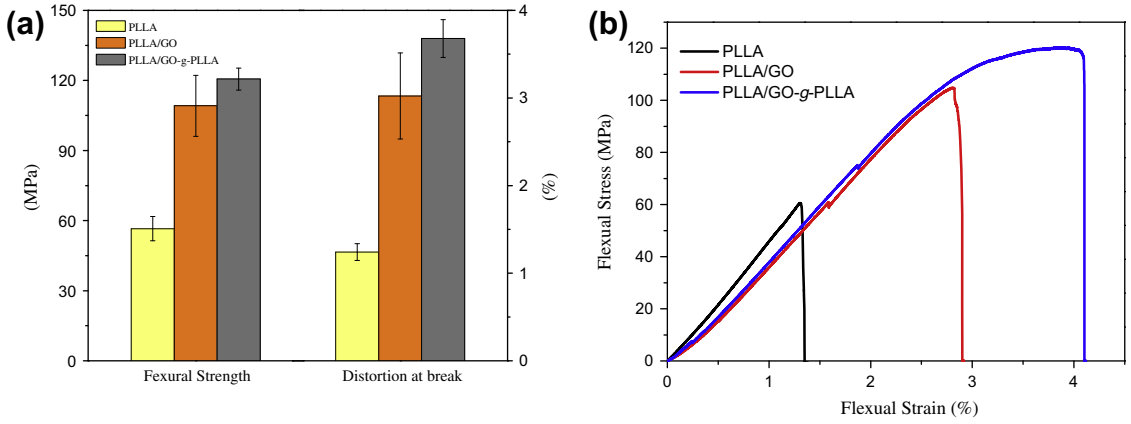

Fig. 11. Absolute value of fexural strength and distortion at break (a) and typical fexural stress–strain curves (b) of PLLA, PLLA/GO and PLLA/GO-*g*-PLLA nanocomposites.

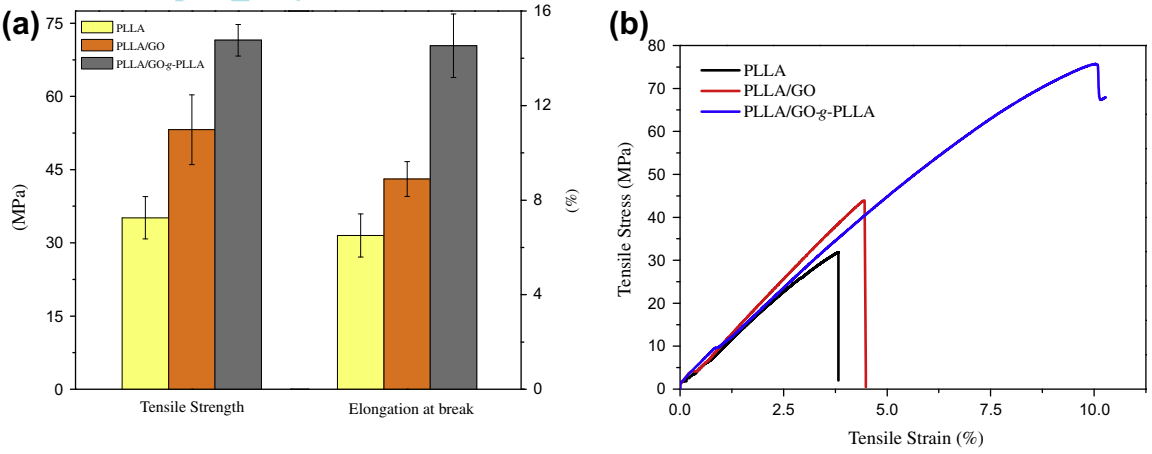

Fig. 12. Absolute value of tensile srength and elongation at break (a) and typical tensile stress–strain curves (b) of PLLA, PLLA/GO and PLLA/GO-g-PLLA nanocomposites.

charges on GO surface can interact effectively with PLLA via hydrogen bonding and electrostatic attraction, as reflected from Fig. 10 and other reports [54,59]. Despite poor dispersion of GO, the addition of it still improved the flexural properties of PLLA in some degree. While in the case of PLLA/GO-*g*-PLLA composites, the flexural properties of PLLA nanocomposites was further improved, which could be attributed to the efficient load transfer between graphene sheets and PLLA matrix. The stable and uniform dispersion of GO-*g*-PLLA in the chloroform solution (as seen in the Figs. 5 and 6) was bound to result in a good dispersion of GO-*g*-PLLA in the PLLA matrix(as reflected in the Fig. 7c), which would favor the stress transfer across the interaction between GO-*g*-PLLA and PLLA matrix [60]. The specific polymer chains on GO surface not only improved the dispersibility of nanofillers but also provided the strong interfacial adhesion between GO-*g*-PLLA and PLLA because the brushed PLLA on surface of GO inserted into PLLA matrix due to same nature of them, which can be reflected from the increase values of T_g and T_m. As a result, significant enhancement of flexural properties of the composites was achieved. The typical stress–strain curves of these nanocompsites were presented in Fig. 11b. As seen in it, the PLLA and PLLA/GO both showed the typical characteristics of brittle material: Hookean (linear) behavior and absence of continuous yielding. As to PLLA/GO-*g*-PLLA, the curve occurred a region of plastic deformation and a higher elongation, which indicated that the addition of GO-*g*-PLLA enhanced the toughness of PLLA.

Fig. 12 showed the averaged tensile properties and typical stress–strain curves. As seen in them, adding both the two types of graphene sheets to PLLA would increase the initial tensile properties of the composites. When GO was added into the PLLA matrix, tensile strength of PLLA/GO nanocomposites increased from 35 MPa of PLLA to 53 MPa (an increase of 51.4%), and the elongation at break increased from 6.50% to 8.91% (an increase of 37.1%). As to PLLA/GO-*g*-PLLA composites, tensile strength of them further increased to 72 MPa (an increase of 105.7%) and elongation at break increased to 14.48% (an increase of 122.8%). As aforementioned, this is due to a matrix stiffening effect induced by nano-sized carbon material reinforcement in PLLA matrix.

In the flexural tests, the breaking strength of PLLA/GO-*g*-PLLA nanocomposites (120 MPa) increased by 10.1% compared with PLLA/GO (109 MPa), while in tensile tests, it increased by 35.8%. This is due to the fact that the tensile failure mechanism in nanocomposites is usually caused by interfacial debonding [61], so the efficient reinforcing effect of functionalized GO performed especially apparent in tensile tests. Good dispersion of GO-*g*-PLLA and strong interfacial interactions between GO-g-PLLA and matrix made a huge contribution to the enhancement effect of GO-*g*-PLLA on the tensile properties of composites.

4. Conclusions

The lyophilized GO, without any further modification, was efficiently covalently functionalized with biocompatible PLLA via one step based on in situ polycondensation of the commercially available L -lactic acid monomer. FTIR and XPS studies indicated that the rich oxygen-containing functional groups on the GO showed active enough for participating the polycondensation of L-lactic acid and thus biocompatible PLLA was successfully grafted onto the surface of GO. TGA results showed that GO could obtain a high grafting rate of PLLA (30.8%) under a moderate condition (as described above). Moreover, the addition of graphene derivatives could facilitate the cold crystallization behavior of PLLA and improved its T_g and T_m values, but had little effect on the crystallinity of PLLA. GO-*g*-PLLA could be well-dispersed in PLLA matrix and exhibited excellent enhancement of mechanical properties of PLLA composites. With only 0.5 wt% loading of GO-*g*-PLLA, LLA/GO-*g*-PLLA composites showed 114.3% and 105.7% increases in flexural and tensile strength compared with neat PLLA, respectively. These excellent properties were due to the homogeneous dispersion, high interfacial area and strong adhesion forces caused by the surface specific functional groups. As one of the most important biocompatible and biodegradable materials, PLLA incorporating with high-performance graphene sheets grant improvement of mechanical performance and may promise multipurpose in PLLA. The route to prepare GO-*g*-PLLA should be favored in industrialization for its short technological process and cheap commercially available raw material.

Acknowledgments

The work was funded by the National Natural Science Foundation of China (11175130), Natural Science Foundation of Tianjin, China (10JCYBJC02300), China Postdoctoral Science Foundation (2012M520578) and the Jiangsu Planned Projects for Postdoctoral Research Funds (1202067C).

References

[1] T. Wang, L.T. Drzal, Cellulose-nanofiber-reinforced poly(lactic acid) composites prepared by a water-based approach, ACS Appl. Mater. Interfaces 4 (2012) 5079–5085.
[2] G. Pandey, E.T. Thostenson, Carbon nanotube-based multifunctional polymer nanocomposites, Polym. Rev. 52 (2012) 355–416.
[3] M. Li, Y.G. Jeong, Poly(ethylene terephthalate)/exfoliated graphite nanocomposites with improved thermal stability, mechanical and electrical properties, Compos. A-Appl. Sci. Manuf. 42 (2011) 560–566.
[4] S.H. Shim, K.T. Kim, J.U. Lee, W.H. Jo, Facile method to functionalize graphene oxide and its application to poly(ethylene terephthalate)/graphene composite, ACS Appl. Mater. Interfaces 4 (2012) 4184–4191.
[5] S. Ansari, A. Kelarakis, L. Estevez, E.P. Giannelis, Oriented arrays of graphene in a polymer matrix by in situ reduction of graphite oxide nanosheets, Small 6 (2010) 205–209.
[6] K. Chrissafis, E. Pavlidou, K.M. Paraskevopoulos, T. Beslikas, N. Nianias, D. Bikiaris, Enhancing mechanical and thermal properties of PLLA ligaments with fumed silica nanoparticles and montmorillonite, J. Therm. Anal. Calorim. 105 (2011) 313–323.
[7] K. Wakabayashi, C. Pierre, D.A. Dikin, R.S. Ruoff, T. Ramanathan, L.C. Brinson, J.M. Torkelson, Polymer-graphite nanocomposites: effective dispersion and major property enhancement via solid-state shear pulverization, Macromolecules 41 (2008) 1905–1908.
[8] S. Stankovich, D.A. Dikin, G.H.B. Dommett, K.M. Kohlhaas, E.J. Zimney, E.A. Stach, R.D. Piner, S.T. Nguyen, R.S. Ruoff, Graphene-based composite materials, Nature 442 (2006) 282–286.
[9] A.H. Castro Neto, F. Guinea, N.M.R. Peres, K.S. Novoselov, A.K. Geim, The electronic properties of graphene, Rev. Mod. Phys. 81 (2009) 109–162.
[10] K. Kalaitzidou, H. Fukushima, L.T. Drzal, Multifunctional polypropylene composites produced by incorporation of exfoliated graphite nanoplatelets, Carbon 45 (2007) 1446–1452.
[11] Y. Sun, C. He, Synthesis and stereocomplex crystallization of poly(lactide)–graphene oxide nanocomposites, ACS Macro Lett. (2012) 709–713.
[12] V.G. Shevchenko, S.V. Polschikov, P.M. Nedorezova, A.N. Klyamkina, A.N. Shchegolikhin, A.M. Aladyshev, V.E. Muradyan, In situ polymerized poly(propylene)/graphene nanoplatelets nanocomposites: dielectric and microwave properties, Polymer 53 (2012) 5330–5335.
[13] T. Ramanathan, A.A. Abdala, S. Stankovich, D.A. Dikin, M. Herrera-Alonso, R.D. Piner, D.H. Adamson, H.C. Schniepp, X. Chen, R.S. Ruoff, S.T. Nguyen, I.A. Aksay, R.K. Prud'homme, L.C. Brinson, Functionalized graphene sheets for polymer nanocomposites, Nat. Nanotechnol. 3 (2008) 327–331.
[14] L. Lei, J. Qiu, E. Sakai, Preparing conductive poly(lactic acid) (PLA) with poly(methyl methacrylate) (PMMA) functionalized graphene (PFG) by admicellar polymerization, Chem. Eng. J. 209 (2012) 20–27.
[15] J.T. Yoon, S.C. Lee, Y.G. Jeong, Effects of grafted chain length on mechanical and electrical properties of nanocomposites containing polylactide-grafted carbon nanotubes, Compos. Sci. Technol. 70 (2010) 776–782.
[16] C.-C. Teng, C.-C.M. Ma, B.-D. Cheng, Y.-F. Shih, J.-W. Chen, Y.-K. Hsiao, Mechanical and thermal properties of polylactide-grafted vapor-grown carbon nanofiber/polylactide nanocomposites, Compos. A Appl. Sci. Manuf. 42 (2011) 928–934.
[17] S.S. Ray, M. Okamoto, Biodegradable polylactide and its nanocomposites: opening a new dimension for plastics and composites, Macromol. Rapid Commun. 24 (2003) 815–840.
[18] Q. Lijun, Q. Jianhui, L. Mingzhu, D. Shenglong, S. Liang, L. Shaoyu, Z. Guohong, Z. Yang, F. Xie, Mechanical and thermal properties of poly(lactic acid) composites with rice straw fiber modified by poly(butyl acrylate), Chem. Eng. J. 166 (2011) 772–778.

[19] Y. Cao, J. Feng, P. Wu, Preparation of organically dispersible graphene nanosheet powders through a lyophilization method and their poly(lactic acid) composites, Carbon 48 (2010) 3834–3839.
[20] J.-H. Yang, S.-H. Lin, Y.-D. Lee, Preparation and characterization of poly(L-lactide)–graphene composites using the in situ ring-opening polymerization of PLLA with graphene as the initiator, J. Mater. Chem. 22 (2012) 10805.
[21] D. Garlotta, A literature review of poly(lactic acid), J. Polym. Environ. 9 (2001) 63–84.
[22] F. Achmad, K. Yamane, S. Quan, T. Kokugan, Synthesis of polylactic acid by direct polycondensation under vacuum without catalysts, solvents and initiators, Chem. Eng. J. 151 (2009) 342–350.
[23] W. Song, Z. Zheng, W. Tang, X. Wang, A facile approach to covalently functionalized carbon nanotubes with biocompatible polymer, Polymer 48 (2007) 3658–3663.
[24] J.T. Yoon, Y.G. Jeong, S.C. Lee, B.G. Min, Influences of poly(lactic acid)-grafted carbon nanotube on thermal, mechanical, and electrical properties of poly(lactic acid), Polym. Adv. Technol. 20 (2009) 631–638.
[25] D.C. Marcano, D.V. Kosynkin, J.M. Berlin, A. Sinitskii, Z. Sun, A. Slesarev, L.B. Alemany, W. Lu, J.M. Tour, Improved synthesis of graphene oxide, ACS Nano 4 (2010) 4806–4814.
[26] K.A. Wepasnick, B.A. Smith, K.E. Schrote, H.K. Wilson, S.R. Diegelmann, D.H. Fairbrother, Surface and structural characterization of multi-walled carbon nanotubes following different oxidative treatments, Carbon 49 (2011) 24–36.
[27] H. Hu, Z. Zhao, Q. Zhou, Y. Gogotsi, J. Qiu, The role of microwave absorption on formation of graphene from graphite oxide, Carbon 50 (2012) 3267–3273.
[28] J. Shen, Y. Hu, M. Shi, X. Lu, C. Qin, C. Li, M. Ye, Fast and facile preparation of graphene oxide and reduced graphene oxide nanoplatelets, Chem. Mater. 21 (2009) 3514–3520.
[29] A.L. Goffin, J.M. Raquez, E. Duquesne, G. Siqueira, Y. Habibi, A. Dufresne, P. Dubois, From interfacial ring-opening polymerization to melt processing of cellulose nanowhisker-filled polylactide-based nanocomposites, Biomacromolecules 12 (2011) 2456–2465.
[30] P.G. Seligra, F. Nuevo, M. Lamanna, L. Famá, Covalent grafting of carbon nanotubes to PLA in order to improve compatibility, Compos. B Eng. 46 (2013) 61–68.
[31] Y. Cao, J. Feng, P. Wu, Alkyl-functionalized graphene nanosheets with improved lipophilicity, Carbon 48 (2010) 1683–1685.
[32] S. Stankovich, D.A. Dikin, R.D. Piner, K.A. Kohlhaas, A. Kleinhammes, Y. Jia, Y. Wu, S.T. Nguyen, R.S. Ruoff, Synthesis of graphene-based nanosheets via chemical reduction of exfoliated graphite oxide, Carbon 45 (2007) 1558–1565.
[33] J.I. Paredes, S. Villar-Rodil, A. Martinez-Alonso, J.M.D. Tascon, Graphene oxide dispersions in organic solvents, Langmuir 24 (2008) 10560–10564.
[34] Y. Si, E.T. Samulski, Synthesis of water soluble graphene, Nano Lett. 8 (2008) 1679–1682.
[35] S. Stankovich, R.D. Piner, S.T. Nguyen, R.S. Ruoff, Synthesis and exfoliation of isocyanate-treated graphene oxide nanoplatelets, Carbon 44 (2006) 3342–3347.
[36] L. Hua, W. Kai, J. Yang, Y. Inoue, A new poly(L-lactide)-grafted graphite oxide composite: facile synthesis, electrical properties and crystallization behaviors, Polym. Degrad. Stab. 95 (2010) 2619–2627.
[37] M. Amirian, A.N. Chakoli, J.H. Sui, W. Cai, Enhanced mechanical and photoluminescence effect of poly(L-lactide) reinforced with functionalized multiwalled carbon nanotubes, Polym. Bull. 68 (2012) 1747–1763.
[38] B. Olalde, J.M. Aizpurua, A. Garcia, I. Bustero, I. Obieta, M.J. Jurado, Single-walled carbon nanotubes and multiwalled carbon nanotubes functionalized with poly(L-lactic acid): a comparative study, J. Phys. Chem. C 112 (2008) 10663–10667.
[39] G.X. Chen, H.S. Kim, B.H. Park, J.S. Yoon, Controlled functionalization of multiwalled carbon nanotubes with various molecular-weight poly(L-lactic acid), J. Phys. Chem. B 109 (2005) 22237–22243.
[40] D.R. Dreyer, S. Park, C.W. Bielawski, R.S. Ruoff, The chemistry of graphene oxide, Chem. Soc. Rev. 39 (2010) 228–240.
[41] T. Maharana, B. Mohanty, Y.S. Negi, Melt–solid polycondensation of lactic acid and its biodegradability, Prog. Polym. Sci. 34 (2009) 99–124.
[42] Y. Li, X.S. Sun, Preparation and characterization of polymer-inorganic nanocomposites by in situ melt polycondensation of L-lactic acid and surface-hydroxylated MgO, Biomacromolecules 11 (2010) 1847–1855.
[43] G.-X. Chen, H.-S. Kim, B.H. Park, J.-S. Yoon, Synthesis of poly(L-lactide)-functionalized multiwalled carbon nanotubes by ring-opening polymerization, Macromol. Chem. Phys. 208 (2007) 389–398.
[44] Y. Sun, C. He, Synthesis, stereocomplex crystallization, morphology and mechanical property of poly(lactide)–carbon nanotube nanocomposites, RSC Adv. 3 (2013) 2219.
[45] L. Chen, Z. Xu, J. Li, Y. Li, M. Shan, C. Wang, Z. Wang, Q. Guo, L. Liu, G. Chen, X. Qian, A facile strategy to prepare functionalized graphene via intercalation, grafting and self-exfoliation of graphite oxide, J. Mater. Chem. 22 (2012) 13460.
[46] M.T. Liu, M.F. Pu, H.W. Ma, Preparation, structure and thermal properties of polylactide/sepiolite nanocomposites with and without organic modifiers, Compos. Sci. Technol. 72 (2012) 1508–1514.
[47] W. Chen, L. Yan, Preparation of graphene by a low-temperature thermal reduction at atmosphere pressure, Nanoscale 2 (2010) 559–563.
[48] M. Fang, K. Wang, H. Lu, Y. Yang, S. Nutt, Covalent polymer functionalization of graphene nanosheets and mechanical properties of composites, J. Mater. Chem. 19 (2009) 7098.
[49] J. Wang, Z. Shi, Y. Ge, Y. Wang, J. Fan, J. Yin, Functionalization of unzipped carbon nanotube via in situ polymerization for mechanical reinforcement of polymer, J. Mater. Chem. 22 (2012) 17663–17670.
[50] J. Feng, W. Cai, J. Sui, Z. Li, J. Wan, A.N. Chakoli, Poly(L-lactide) brushes on magnetic multiwalled carbon nanotubes by in-situ ring-opening polymerization, Polymer 49 (2008) 4989–4994.
[51] C. Aoneng, L. Zhen, C. Saisai, W. Minghong, Y. Zhangmei, C. Zhengwei, C. Yanli, W. Shufeng, G. Qihuang, L. Yuanfang, A facile one-step method to produce graphene-CdS quantum dot nanocomposites as promising optoelectronic materials, Adv. Mater. 22 (2010) 103–106.
[52] H. Adeli, S.H.S. Zein, S.H. Tan, H.M. Akil, A.L. Ahmad, Synthesis, characterization and biodegradation of novel poly(L-lactide)/multiwalled carbon nanotube porous scaffolds for tissue engineering applications, Curr. Nanosci. 7 (2011) 323–332.
[53] S. Solarski, M. Ferreira, E. Devaux, Characterization of the thermal properties of PLA fibers by modulated differential scanning calorimetry, Polymer 46 (2005) 11187–11192.
[54] L. He, J. Sun, X. Wang, X. Fan, Q. Zhao, L. Cai, R. Song, Z. Ma, W. Huang, Unzipped multiwalled carbon nanotubes-incorporated poly(L-lactide) nanocomposites with enhanced interface and hydrolytic degradation, Mater. Chem. Phys. 134 (2012) 1059–1066.
[55] A. Leszczynska, K. Pielichowski, Application of thermal analysis methods for characterization of polymer/montmorillonite nanocomposites, J. Therm. Anal. Calorim. 93 (2008) 677–687.
[56] J.W. Suk, R.D. Piner, J. An, R.S. Ruoff, Mechanical properties of mono layer graphene oxide, ACS Nano 4 (2010) 6557–6564.
[57] R. Sengupta, M. Bhattacharya, S. Bandyopadhyay, A.K. Bhowmick, A review on the mechanical and electrical properties of graphite and modified graphite reinforced polymer composites, Prog. Polym. Sci. 36 (2011) 638–670.
[58] Y. Lin, K.-Y. Zhang, Z.-M. Dong, L.-S. Dong, Y.-S. Li, Study of hydrogen-bonded blend of polylactide with biodegradable hyperbranched poly(ester amide), Macromolecules 40 (2007) 6257–6267.
[59] J. Liang, Y. Huang, L. Zhang, Y. Wang, Y. Ma, T. Guo, Y. Chen, Molecular-level dispersion of graphene into poly(vinyl alcohol) and effective reinforcement of their nanocomposites, Adv. Funct. Mater. 19 (2009) 2297–2302.
[60] K.-Y. Lee, P. Bharadia, J.J. Blaker, A. Bismarck, Short sisal fibre reinforced bacterial cellulose polylactide nanocomposites using hairy sisal fibres as reinforcement, Compos. A Appl. Sci. Manuf. 43 (2012) 2065–2074.
[61] D.B. Marshall, B.N. Cox, Tensile fracture of brittle matrix composites: influence of fiber strength, Acta Metall. 35 (1987) 2607–2619.